ORIGINAL ARTICLE

Structure and physical properties changes of Fe-based amorphous alloy induced by Joule-heating

Yulia Nykyruy[1] · Yuriy Kulyk[1] · Stepan Mudry[1] · Vitaly Prunitsa[1] · Anatoliy Borysiuk[2]

Abstract

Electrical current annealing based on the Joule-heating technique, known also as the thermal electrical resistivity method, was applied for nanocrystallyzation of the $Fe_{73.5}Nb_3Cu_1Si_{15.5}B_7$ amorphous ribbon. The feature of the Joule-heating technique is high heating rates of the material internal volume that in the case of amorphous alloys causes the evolution of the metastable amorphous state. Structure transformation was investigated by the X-ray diffraction method, which allows obtaining the phase composition of the material as well as nanograin size. The nanocrystalline phases that precipitate during current annealing are Fe_3Si and hexagonal phase with a nanoscale grain size, the average value of which tends to depend on annealing duration as well as applied voltage and varies in the range of 10–200 nm. Field-emission scanning electron microscopy was used to investigate the surface topology and nanograins, and at some samples, petal-like structures were observed on the ribbon's surface after the Joule-heating technique application. Saturation magnetization and microhardness were studied in relation to electrical current parameters, and optimal values were observed for its improvement. Obtained results could be helpful for controlling the conditions of the formation of fully or partially nanocrystalline structured materials from amorphous ribbons based on Fe-Si-B-Nb-Cu.

Keywords Fe-based amorphous alloy · Nanocrystallization · Electrical current annealing · Joule-heating · Magnetic properties

Introduction

Amorphous metal alloys (AMA), also known as metallic glass, have practical applications, first of all, due to unique magnetic properties, good mechanical behaviour, and high corrosion resistance. Nowadays, Fe-based amorphous and nanocrystalline alloys are widely used in magnetic conductors of various inductive components (transformers, sensor elements, cores, choke coils, magnetic screens/ shielding, etc.) (Hasegawa 2004; Ackland et al. 2018; Jifeng et al. 2022). It is known that the formation of α-Fe(Si) nanocrystals in these alloys improves their magnetic properties. After the appropriate thermal treatment, the volume fraction of the nanocrystalline phase in these alloys varies in the range

up to 80%, with an average size of nanocrystals from 10 to 12 nm (Pogorily et al 2019). It is estimated that the use of new FeSiB-based nanocrystalline alloys for transformer cores to reduce giant power losses in the present expectation of high efficiency and improved performance of hybrid/electric vehicle engines will significantly reduce costs (Nosenko 2015). As green, energy-saving, and environmentally friendly materials, their application fields have more possibilities (Jifeng et al. 2022). Alloys based on Fe-Si-B-Nb-Cu, known as Finemet, are obtained from the Fe-Si-B system by a minor addition of Cu and Nb. High soft magnetic properties in these alloys are usually caused by the precipitation of nanocrystalline α-Fe dispersed in an amorphous matrix. The Finemet-based alloys are attractive as soft magnetic materials due to the opportunity for further improvement, which makes the alloys suitable for electric power applications and others. The development of modern technologies and new materials is based on fundamental studies that determine material formation, as well as the correlation between physical properties and structure. It is well known that the properties of amorphous materials are very sensitive to internal

✉ Yulia Nykyruy
 yuliya.nykyruy@lnu.edu.ua

1 Metal Physics Department, Ivan Franko National University of Lviv, Lviv, Ukraine

2 Department of Applied Physics and Nanomaterial Science, Lviv Polytechnic National University, Lviv, Ukraine

range ordering and phase structure, which, in turn, can be modified by different techniques. The techniques based on the Joule heating, also known as thermal electrical resistivity method, attract attention due to their intrinsic conceptual simplicity (Allia et al. 1994). Joule-heat annealing is the use of an electric current to generate heat for the material heating. The so-called technique of dc Joule-heating involves the controlling thermal conditions by varying an electrical current and times. Joule-heating as a technique for crystallization in an amorphous metal alloy was applied in (Gupta et al. 2007a, b; Okulov et al. 2015; Bednarčík, et al. 2020). The feature of the Joule-heating technique is high heating rates of the material internal volume that in the case of amorphous alloys causes the evolution of the metastable amorphous state. Variation of the heat-treatment parameters enables obtaining either fully crystalline composites with different volume fraction or composites with uniformly distributed micro-crystals in the glassy matrix. Obviously, as the annealing time or current density increases, the volume fraction of the crystalline phase also increases; however, due to non-equilibrium thermodynamic conditions during rapid annealing and metastable phases in AMAs, this method is of interest for researchers both from fundamental and application point view. The study of the crystallization kinetics in strongly non-equilibrium conditions, which are difficult to create by traditional methods of processing amorphous metal materials, is a relevant problem. In recent years, the method of Joule-heating of amorphous alloys has received little attention, so this method remains little studied in terms of its application to the structuring and improvement of the properties of AMA. In particular, we are interested in the features of AMA crystallization at high heating rates. At the same time, the amorphous Fe-Si-B-Nb-Cu alloy is well-studied in traditional processes, and a lot of literature data makes it possible to verify the reliability of the obtained results and makes it possible to draw correct conclusions about the influence of high heating rates on nanocrystallization processes.

Materials and methods

Amorphous alloy $Fe_{73.5}Nb_3Cu_1Si_{15.5}B_7$ was obtained in the form of a ribbon 30 μm thick and 20 mm wide. The single-roller melt-spinning method was used for ribbon manufacturing that involves casting molten metal by jetting it onto a rotating drum in the form of 20–30 μm thick ribbon (Nosenko et al. 2008). To induce structure transformation, Joule heat annealing was applied to the amorphous ribbon at an alternating electrical current, different voltage, and time. The scheme of Joule-heating is shown in Fig. 1, where AT—autotransformer, CT—power transformer, A1 (V1) is an ammeter (voltmeter) for measuring current and voltage
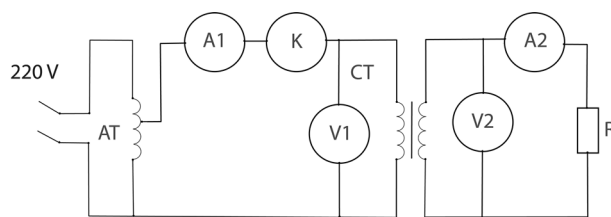
Fig. 1 Scheme of Joule-heating

in the primary winding of the CT, A2 (V2) is an ammeter (voltmeter) for measuring current and voltage in the secondary winding of the CT, K is a contactor, R is a sample of the ribbon connected to the outputs of the CT secondary winding. The amorphous ribbon was divided into samples about 25 mm long. The current density was varied in the range of 1.5–2.8 A/m² while the annealing duration was in the range of 3–120 s. The evolution of the amorphous structure was induced by passing an alternating current through the material in an air atmosphere. The experiments were separated into four types: (1) voltage 1.5 V and annealing duration 15, 30, 45, 60, and 120 s; (2) voltage 1.9 V, annealing duration 10, 15, and 60 s; (3) voltage 2.2 V, annealing duration 3, 5, and 10 s; (4) annealing duration 20 s, voltage 1.2, 1.4, 1.6, 1.7, 1.8, 1.9, 2.0, and 2.1 V.

Structure changes were studied using the backscattered X-ray diffraction (XRD) method (Cu-Kα radiation, $\lambda = 1.5418$ Å). Identification of crystalline phases, which precipitates in the alloy, was performed analysing reflexes on the X-ray intensity curve. So, phases were determined by the interpretation of the diffraction peaks positions. An observed diffraction peaks were reproduced by fitting partial diffraction peaks by Lorentzians using the OriginLab software, and the full width at half maximum (FWHM) of the fitted peak was used for the estimation of an average size of regions of coherent scattering from the appropriate phase. Interplanar distance d (spacing parameter) of the crystalline structure was determined by the following formula:

$$d = \frac{\lambda}{2\sin\theta} \tag{1}$$

where λ is the wavelength of the X-ray, 2θ is the scattering angle. The average grain size of crystallites (L_{cr}) was determined using formula (Langford and Wilson 1978):

$$L_{cr} = \frac{\lambda}{\beta\cos\theta} \tag{2}$$

where $\beta = B - b$; B and b—full width at half maximum (FWHM) for the investigated and reference samples respectively.

Magnetic measurements were performed using a vibrating sample magnetometer. The ribbon surface was studied

by a field emission scanning electron microscopy (FESEM), using the Hitachi S-4100 microscope with a secondary electron detector. Microhardness (H_V) of the as-quenched and annealed samples was determined using hardness measuring unit PMT-3. Measurements were carried out at loading on sample 165 g for 15 s. Microhardness was calculated by the formula:

$$H_V = 1854 \frac{P}{a^2} \tag{3}$$

where a is the indentation diagonal, and P—the load applied to the indenter. The microhardness was measured based on 10 indenter prints with the following averaging of results.

Results and discussion

Amorphous metal alloys are conductive materials. However, due to disordered structure, their conductivity is lower than that of crystalline analogous. It is known, at low temperatures the resistance of metals is determined by lattice defects and impurities, and is called the residual resistance ρ_0. As the temperature rises, thermal fluctuations of the lattice appear and intensify, and the resistance of many metals increases. Because the residual resistance is caused by impurities and defects of crystalline structure, then any processes that increase the density of the lattice defects lead to an increase of ρ_0. Such processes include quenching from a melt that results in the disordered structure of a material. Therefore, the electrical resistance of amorphous metal alloys is 2–3 times greater than the electrical resistance of the corresponding crystalline alloys. A much higher value of the resistance of rapidly quenched alloys, in comparison with crystalline alloys, is the result of a strong influence of chemical and configurational disorder on the free path length of electrons. At the same time, the temperature dependence of the electrical resistance of AMA is almost an order of magnitude weaker than that in the crystalline state (Plevachuk et al. 2014).

According to Joule-Lenz law, heat is generated in a conductor through which a current flows. Since the ribbon sample was in an air, a part of the heat was dissipated due to convection and radiation heat losses, and only a part of the generated heat was spent on heating the sample. The heat balance equation can be written as follows:

$$Q = Q_1 + Q_2 + Q_3 \tag{4}$$

where Q is the heat released in the conductor due to the flow of alternating current; Q_1 is the heat spent on heating the conductor in the temperature interval (T_0, T); Q_2 and Q_3 are the heat released due to convective and radiation heat exchange respectively. According to Joule's Law the heat generated due to the flow of current is:

$$dQ = \frac{U^2}{2R} d\tau \tag{5}$$

where R is the resistance, U is the applied voltage and τ is time. The heat spent on heating can be calculated by the formula:

$$dQ_1 = mcdT \tag{6}$$

where m is mass, that can be obtained as $m = \rho V$, here ρ – is specific density, V is sample volume and c is heat capacity, T is temperature. The heat released due to convective heat exchange can be calculated following the next formula:

$$dQ_2 = k(T)S(T - T_0)d\tau \tag{7}$$

where $k(T)$ is heat transfer coefficient, S– surface area. The heat released due to radiation heat exchange can be calculated following the formula:

$$dQ_3 = \varepsilon S(T^4 - T_0^4)d\tau \tag{8}$$

where ε is the emissivity of the grey body, and was considered as $\varepsilon = 0.5$.

$$\rho VcdT = \left[\frac{U^2}{2R} - k(T)S(T - T_0) - \varepsilon S(T^4 - T_0^4) \right]d\tau \tag{9}$$

$$T = \frac{1}{\rho Vc} \int_{T_0}^{T} \left[\frac{U^2}{2R} - k(T)S(T - T_0) - \varepsilon S(T^4 - T_0^4) \right]d\tau \tag{10}$$

Heat capacity of $Fe_{73.5}Nb_3Cu_1Si_{15.5}B_7$ alloy was taken as $c = 560$ J/kg*K and specific density was defined as an average value based on the literature data for similar alloy, $\rho = 7.35$ kg/m^3 (Shi et al 2020; Ma et al. 2022). Calculated parameters of the Joule-heating process are shown in Table 1 and the calculated temperature changes and heating rates of the samples in Fig. 1a and b. Convection losses become significant at high temperatures; the temperature dependence of the convection heat transfer coefficient is shown in Fig. 1c. Due to convection losses, the heating rates slow down and

Table 1 Applied voltage (U), electrical current (I), current density (J), maximum heating rate ($\Delta T/t$), maximum temperature of the sample (T_s), durations of current annealing (t)

U, V	I, A	J, 10^6 A/m^2	$\Delta T/t$, K/s	T_s, K	t, s
1.5	11.4	19.0	71.7	823.3	15, 30, 45, 60, 120
1.9	14.4	24.1	116.1	943.2	10, 30, 60
2.2	16.7	27.8	154.7	1024.3	3, 5, 10

temperature achieves its maximum value. According to our calculation, the temperature of the samples increases rapidly and then achieves some maximum value, which depends on the applied voltage. Such heating results in structural transformation that was convenient for metastable amorphous structure (Fig. 2).

The XRD study of amorphous structure evolution under the applied voltage of $U = 1.5$ V is shown in Fig. 3a. On the background of an amorphous halo, the appearing of small but clear reflexes can be seen, which corresponds to the silicide Fe_3Si. The intensity of the reflexes increased with time increasing, indicating the increase in the crystalline phase content. According to the calculations for the first 15 s the temperature of the sample (T) had raised up to the 806.7 K. This temperature is close to the first crystallization peak of Finemet type alloys on DSC—curves, that is related to the primary precipitation of bcc-Fe(Si) phase (Sun et al. 2000; Mudry et al. 2010a, b). The temperature–time function for

$U = 1.5$ V reached its maximum value of 823.3 K at 20 s, and further annealing process was realized at the stable temperature. Under this condition, the partial devitrification of the amorphous phase occurred accompanied by nanocrystallization of Fe_3Si. The content of the nanocrystalline phase reached a value of about 30% at 120 s.

The XRD curves for the sample annealed under applied voltage of 1.9 V and 2.2 V indicate crystallization of the metastable hexagonal phase (H-phase), rhombohedral distortion of α-Mn structure, in addition to the Fe_3Si phase (Fig. 3b and c). It is worth noting that in finemet-type alloys the structure transformation from an amorphous to a crystalline state occurs in two stages: primary crystallization of α-Fe(Si) and secondary crystallization of Fe-B phases (Mudry et al. 2007). The temperature of the secondary crystallization for the Fe-Si-B-Nb-Cu is around 900–950 K (Barandiaran 2003; Wang et al. 2016). This temperature range is close to the calculated values of the temperature at
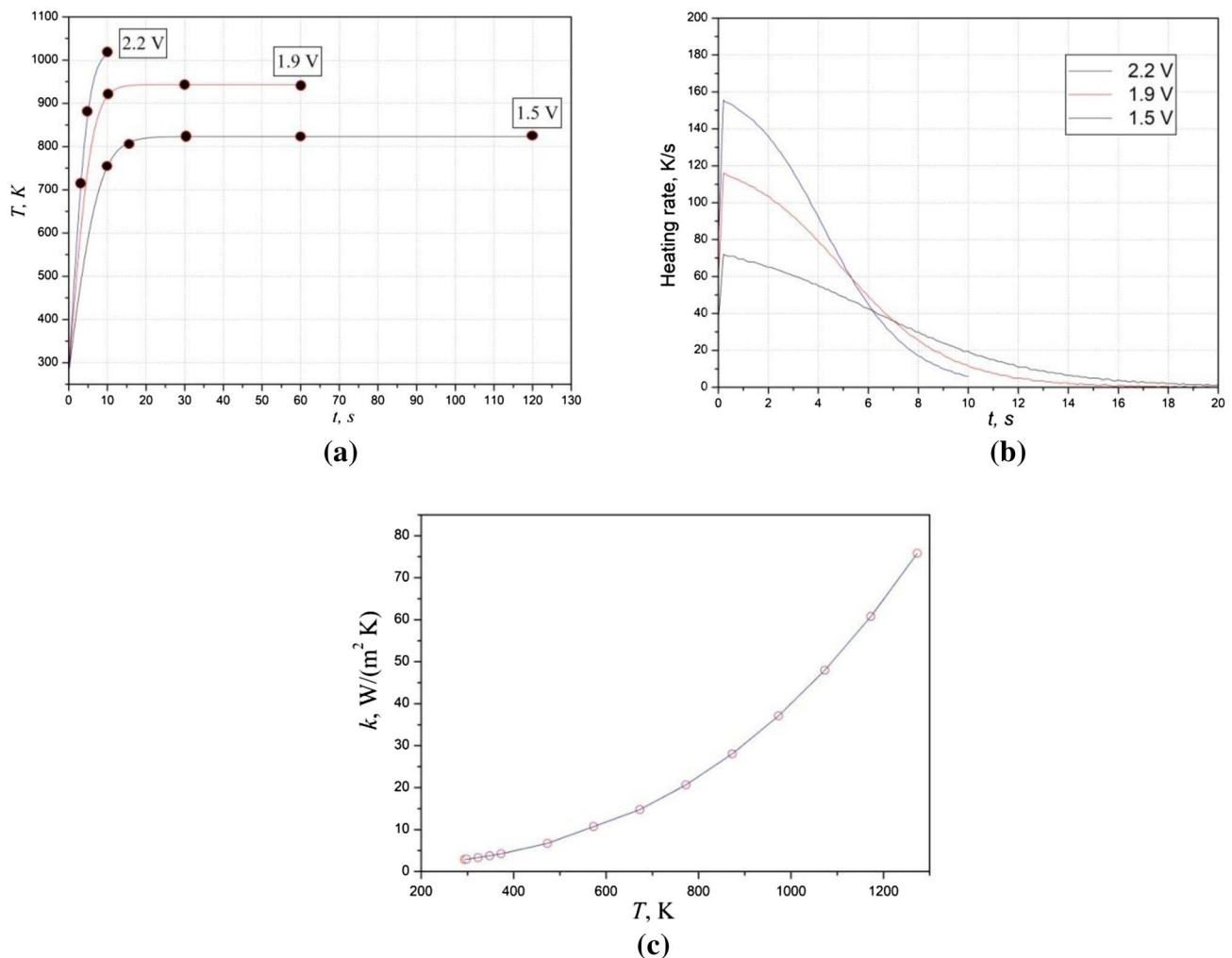
Fig. 2 Temperature of the samples as the function of annealing duration (**a**), heating rates as function of annealing duration (**b**), the temperature dependence of the convection heat transfer coefficient (**c**)
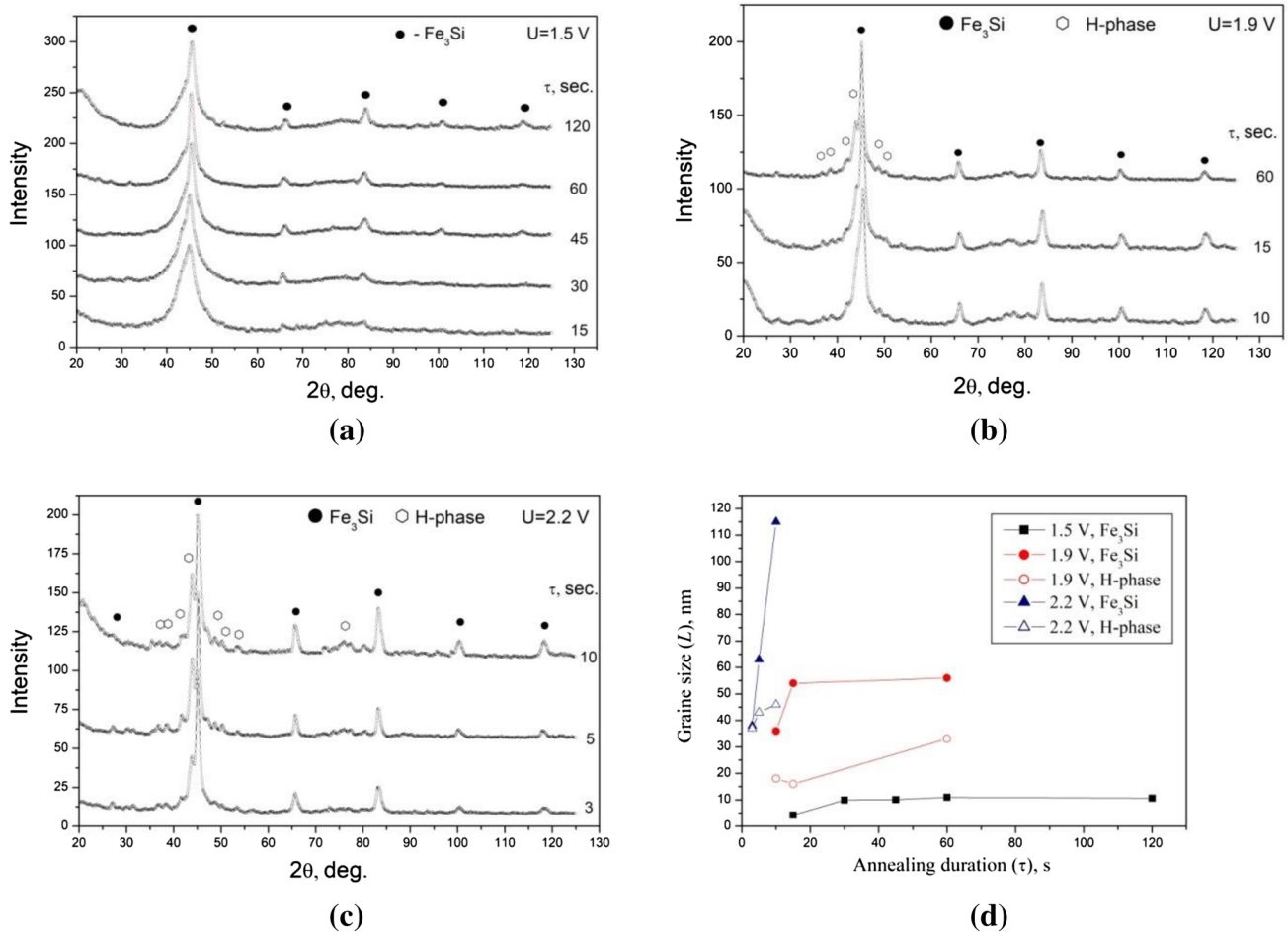
Fig. 3 Diffraction patterns of the ribbon after applied voltage 1.5 V (**a**), 1.9 V (**b**), 2.2 V (**c**) during different duration, and average grain size vs. annealing duration (**d**)

1.9 V and 2.2 V (Table 1). However, no boride phases were detected in the diffraction patterns. It is worth noting that, as evidenced by the DSC results, the temperatures of the first and second peaks increase with the heating rate increasing, hence the phase transitions shift more towards higher temperatures the higher the heating rate is (Boichyshyn et al. 2017; Shihab et al. 2020). Our calculations (Fig. 1c) showed fast and nonequilibrium heating rates for the current annealing modes under consideration. So we can assume that this is the cause of change in the typical mechanism of crystallization. Therewith, the H-phase was detected previously in laser-induced crystallization of the same alloy under laser exposure of 0.1–1.0 s (Nykyruy et al. 2020, 2018). This phase was described as primary crystallization phase in $Fe_{80}Nb_{10}B_{10}$ (Imafuku et al. 2000) and consisted of the Frank-Kasper coordination polyhedra, which are closely related to the local structure in amorphous alloy (Ohnuma et al. 1993). At higher temperature this metastable H-phase disintegrates into Fe_3B (orthorhombic) and Fe_2B. The H-phase precipitation is sensitive to local B distribution.

It can be assumed that the H-phase is crystallized under the condition of non-equilibrium and short-term heating–cooling to temperatures about the beginning of secondary crystallization. An average grain size (L) of the Fe_3Si and H-phase was estimated on the basis of FWHM of the main maximum of the XRD curve and the time dependence of the grain size is shown in Fig. 3d. It can be seen that for the samples A L does not increase with time, after the reaching value of 10–11 nm. So, the processes of nucleation prevailed over the process of growth of crystallites, and the content of the crystalline phase increased due to the formation of new nuclei, and not due to the growth of previously formed ones. Such crystallization process contributes to the formation of a fine nanostructure. At higher voltage (1.9 and 2.2 V) the average grain size increases with time increasing indicating the two mechanisms of structure crystallization: the formation of new nuclei and the growth of previously formed nanocrystallites.

According to the calculations for sample A, which was annealed at 1.5 V (Fig. 1a), the temperature remained

unchanged almost at all annealing duration remaining isothermal conditions. In order to more deeply analyse, the crystallization process was studied within the framework of the theory of nucleation and growth. The theoretical basis for the description of isothermal crystallization of glasses involving both nucleation and growth was formulated mostly by Johnson, Mehl, and Avrami (Málek 1995; Fanfoni and Tomellini 1998). In its basic form, the theory describes the time dependence of the fractional extent of crystallization, $X(t)$. The resulting equation is known as the Johnson–Mehl–Avrami (JMA) equation:

$$X(t) = 1 - \exp(-[K(I, u)t]^n) \qquad (11)$$

where $K(I, u)$ is a rate constant depending on the nucleation (I) and the crystal growth (u) rates, n- the kinetic index (Avrami exponent) which reflects the growth dimensionality. The Avrami exponent n is often evaluated based on the so-called double-logarithm function. Using a double logarithmic coordinates, Eq. 11 is transformed to:

$$\ln(-\ln(1 - X)) = \ln K(T) + n\ln(t) \qquad (12)$$
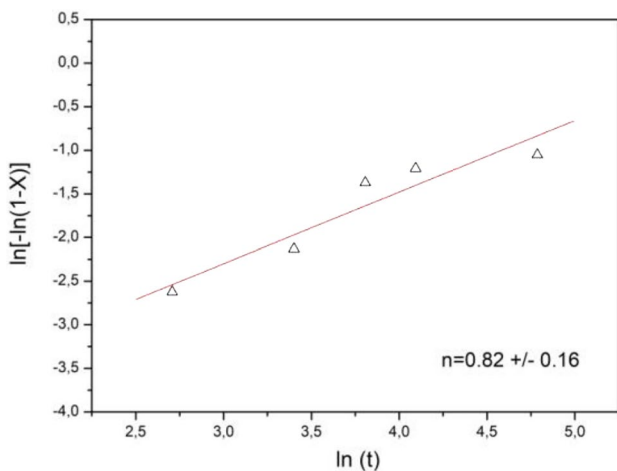
Fig. 4 Avrami plot of the $Fe_{73.5}Nb_3Cu_1Si_{15.5}B_7$ amorphous ribbon under applied voltage 1.5 V

Based on Eq. 12 the Avrami plot was build, and is shown in Fig. 4. The time dependence of the nanocrystal volume fraction for the investigated sample is close to a linear function the slope of which corresponds to Avrami exponent. So, based on Avrami plot, the Avrami exponent was defined as $n = 0.82 \pm 0.16$. The value of n reflects the various mechanisms of nucleation and growth prevalent during the progress of the crystallization process (Paul et al. 2018). In most cases, the Avrami exponent for Fe-Si-B-Nb-Cu amorphous alloys acquires a value in the range 1–4 (Barandiaran 2003; Lashgari et al. 2015; Rezaei-Shahreza et al. 2017; Mudry et al. 2010a, b). However, Avrami exponent values much less than one ($n < 1$) were reported in the studies of the Fe-Nb-Cu-Si-B alloys' crystallization behaviours, which were conducted by the thermal electrical resistivity method (Mitra et al. 1998). According to Paul et al. (2018), $n < 1.5$ can be interpreted as growth of pre-existing nuclei. Due to the increase of Nb in the amorphous matrix, which inhibits the growth of grains of Fe_3Si, the growth rate of nanocrystallites drops significantly that correlates with the grain size versus duration at 1.5 V (Fig. 3d).

The Johnson–Mehl–Avrami equation is frequently used for the analysis of non-isothermal crystallization kinetics, although this theoretical model has limited applicability for non-isothermal transformations. Therefore, the analysis of other samples' crystallization behaviour through the JMA model needs verification of the JMA model's suitability/applicability (Svoboda 2021). Actual verification of the physicochemical conditions, for which the JMA formalism was derived, is rather complicated and laborious and requires extra analysis. Structural parameters of $Fe_{73}Si_{15.5}B_{7.5}Nb_3Cu_1$ ribbon samples annealed at 1.9 and 2.2 V calculated using XRD analysis method are summarized in Tables 2 and 3.

Since structure transformation depends on temperature as well as on duration we used two approaches for inducing structure changes – changing of duration of current annealing at definite voltage (1.5 V, 1.9 V, 2.2 V) and changing of voltage at definite duration of 20 s. For studying the effect of voltage value on the crystallization process at 20 s annealing duration, we choose voltage range of 1.2—2.1 V. Higher values of voltage result in ribbon destroying. Diffraction patterns of the heated ribbon are shown in Fig. 5a

**Table 2** Structure parameters of $Fe_{73}Si_{15.5}B_{7.5}Nb_3Cu_1$ sample ($U = 1.9$ V)

No.	Annealing duration, s	Unit cell parameters, Å		Average grain size, nm	
		Fe_3Si	H-phase	Fe_3Si	H-phase
1	10	$a = 5.6744 \pm 0.0006$	$a = 12.3520 \pm 0.0018$ $c = 7.6797 \pm 0.0014$	36.0 ± 3.5	18.0 ± 2.0
2	15	$a = 5.6799 \pm 0.0006$	$a = 12.3466 \pm 0.0014$ $c = 7.7049 \pm 0.0010$	56.0 ± 6.0	16.0 ± 2.0
3	60	$a = 5.6823 \pm 0.0006$	$a = 12.3280 \pm 0.0012$ $c = 7.7103 \pm 0.0010$	54.5 ± 5.0	33.0 ± 3.5

Table 3 Structure parameters of Fe$_{73}$Si$_{15.5}$B$_{7.5}$Nb$_3$Cu$_1$ sample ($U = 2.2$ V)

No.	Annealing duration, s	Unit cell parameters, Å		Average grain size, nm	
		Fe$_3$Si	H-phase	Fe$_3$Si	H-phase
1	3	$a = 5.6570 \pm 0.0007$	$a = 12.2710 \pm 0.0015$ $c = 7.6862 \pm 0.0010$	38.0 ± 4.0	37.5 ± 4.0
2	5	$a = 5.6795 \pm 0.0006$	$a = 12.3170 \pm 0.0011$ $c = 7.7289 \pm 0.0008$	63.0 ± 6.0	46.0 ± 4.5
3	10	$a = 5.6803 \pm 0.0007$	$a = 12.3475 \pm 0.0015$ $c = 7.6802 \pm 0.0011$	115.0 ± 10.0	43.0 ± 4.0
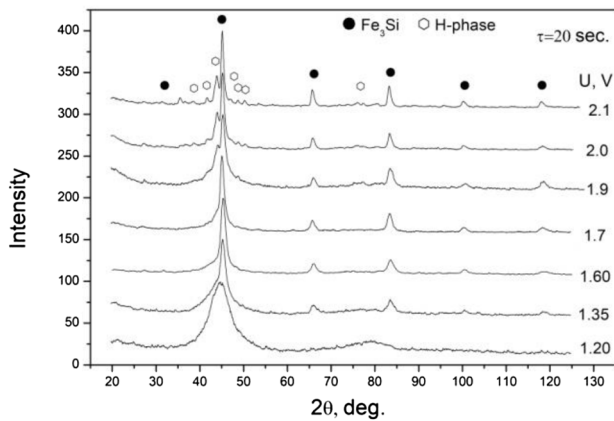
(a)
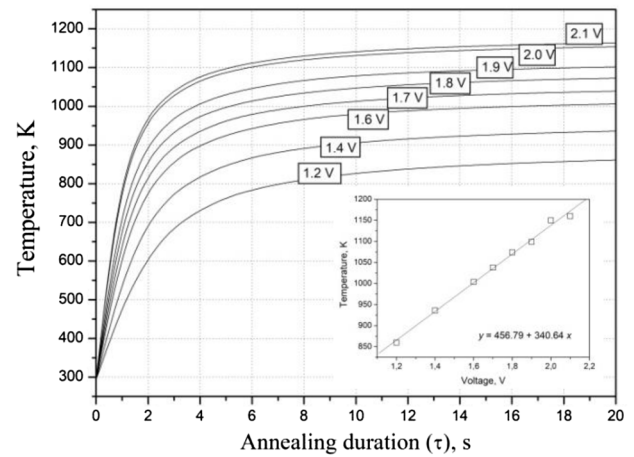
(b)
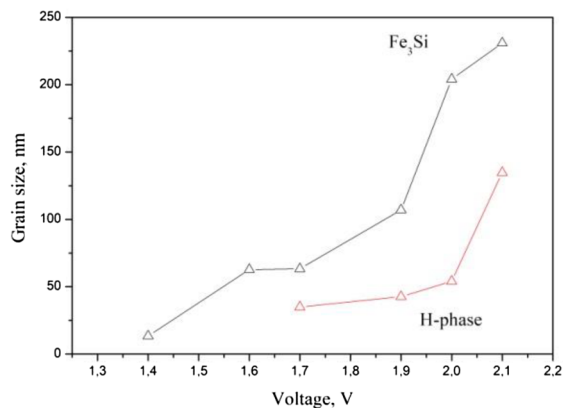
(c)
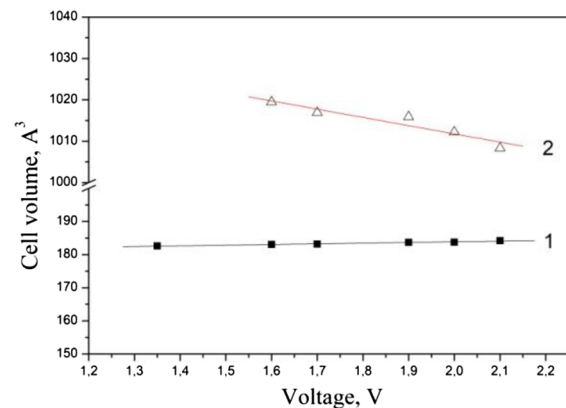
(d)

Fig. 5 Diffraction patterns of the ribbon after applied voltage during time 20 s (**a**), temperature of the samples at different voltages as the function of annealing duration (**b**), the average grain size vs. voltage (**c**), volume of the unit cell of the Fe$_3$Si (1) and H-phase (2) depending on the applied voltage (**d**)

and temperature of the samples as functions of annealing duration in Fig. 5b. Reflexes obtained on the XRD-curves correspond to phase Fe$_3$Si, while the voltage is 1.2–1.6 V corresponding to temperature of 700–850 K. Reflexes of the H-phase are visible at curves for applied voltage of 1.7–2.1 V corresponding to the temperature 883–1023 K. With voltage increasing in range 1.2–1.9 V, the average grain size of the Fe$_3$Si and H-phase increased in range 50–100 nm, while at voltages 1.9–2.1 V the grain size increased drastically up to about 150–200 nm (Fig. 5c). The cell volume for Fe$_3$Si slightly increased, and for H-phase decreased (Fig. 5d).

Microscopic studies of the ribbon samples revealed surface structure changes after current annealing. Amorphous

materials obtained by the method of quenching from the melt have a smooth and uniform structure that resembles the structure of a liquid (Mudry et al. 2015, Nykyruy and Mudry 2020). The output of the study of such a structure using SEM in the mode of secondary electrons is the uniform without any contrast image (Fig. 6a and b). As a result of crystallization, nanocrystallites are formed in the amorphous matrix, which can be detected by a microscope at the nanoscale level. In particular, Fig. 6c and d shows the nanograin structure of the surface of the sample after annealing at 1.9 V (c and d) and 2.1 V (e and f) during 20 s. The grain size distribution analysis was conducted using ImageJ and Origin-Lab software (insert to Fig. 6d). The distribution is fitted by the Gaussian curve; the average grain size is determined as 51.1 nm and standard deviation as 81.2. The obtained result correlates with the data obtained by the XRD method, where the grain size was defined as 50–100 nm (Fig. 5c).

The images in Fig. 6e and 6f show petal-like structures that consist from a randomly oriented nanopetals of about 50 nm thick and 500 nm length. This structure is similar to that obtained in amorphous Co-based alloy after heat treatment (Nykyruy et al. 2022). In some cases petals are grouped into microflowers. A novel class of hierarchical flower-like nano and microparticles in Ag, Cu, Co, Mn was reported by Cai et al. (2019), Kumar et al. (2020), Ma et al. (2019) and others. Formation of such structure is considered as a self-assembled process (Parveen and Cho 2016). Petal-like structure is a kind of 3D porous structure and has large surface area, which can benefit for the application in catalysts and optoelectronic devices such as solar cells, in sensor application, as an excellent lightweight microwave absorption material (Sheshanath et al. 2020, Sheng et al. 2011, Kumar et al 2020). The flower-like structure contained numerous very thin fakes, with layer spacing appropriate for electromagnetic scattering. All this intensify interest in continuing our research on the nanostructuring of amorphous metals alloys.

Samples that were annealed for 20 s at the voltage range of 1.2–2.1 V were studied by a vibrating sample magnetometer and initial magnetization curves were obtained (Fig. 7a). The relative magnetization (σ/σ_s) increased with increasing magnetic field strength and reached saturation in fields up to 50 kA/m. A change in the applied annealing voltage affects the shape of the magnetization curve and the saturation magnetization. These changes reflect the processes of structural transformations. In particular, saturation magnetization is sensitive to the material composition and is not sensitive to the change in grain size.

The saturation magnetization dependence on the voltage is shown in Fig. 7b. The lowest value of the saturation magnetization was observed for the untreated as-quenched sample, 136 A/m²kg. Current annealing has lead to an increase in saturation magnetization. The highest value of saturation magnetization, 165 A/m²kg, was recorded for the sample after annealing at 1.6 V. The saturation magnetization is called primary or structurally insensitive magnetic property because its values are determined by the very nature of the ferromagnetic phase (crystal lattice, electronic structure of atoms, chemical composition of the phase). This causes a weak dependence of this characteristic on the elastic stresses, shape, and particle size of the ferromagnetic phase in the alloy. It follows that the changes in magnetization are not related to the growth of the particles, but due to changes in the chemical composition of phases and their crystal structure. Such changes in physical properties are associated with the formation of crystalline phases. In particular, as shown by the results of XRD research, annealing at 1.6 V for 20 s leads to the formation of bcc -Fe(Si) nanocrystals distributed in an amorphous matrix. Increasing the voltage to 1.7 V causes the formation of a nanocrystalline H-phase, and as a result, the saturation magnetization has decreased. One of the purposes of a research into new alloy compositions is increasing the saturation magnetization to a value close to the value of pure α-Fe, while maintaining almost zero magnetostriction. Saturation magnetization is related to permeability as:

$$\mu_e = \frac{M_s^2}{2\mu_0 K_u},$$

where μ_e—permeability, M_s^2—saturation magnetization, μ_0—magnetic constant, K_u—anisotropy constants. In our case, we are dealing with small ferromagnetic crystals connected by exchange interactions, with a small coercive force and at the same time high permeability, which is a consequence of the smoothing effect of the exchange interaction for structural correlation lengths much smaller than the width of the walls domains.

The microhardness of the alloy was defined according to formula 3, where a is the diagonal of the print of the indenter. Loading on a sample of 165 g corresponds to load $P = 1.5$ H. Load on sample was chosen so that the condition that the print's diagonal should be smaller than the thickness of the material was fulfilled. Defined values of microhardness are shown in Fig. 8. For the as-quenched sample, the microhardness was 10.6 GPa and reached its highest value of 13.8 after annealing at 1.7 V. This value of microhardness is a bit higher than that for steel 40Kh after various treatments, 8–9 GPa (Kyryliv, et al. 2022) Increasing the voltage to 1.7 V causes the formation of a nanocrystalline H-phase, and as a result, microhardness has increased due to fine nanocrystallization of the residual amorphous phase.
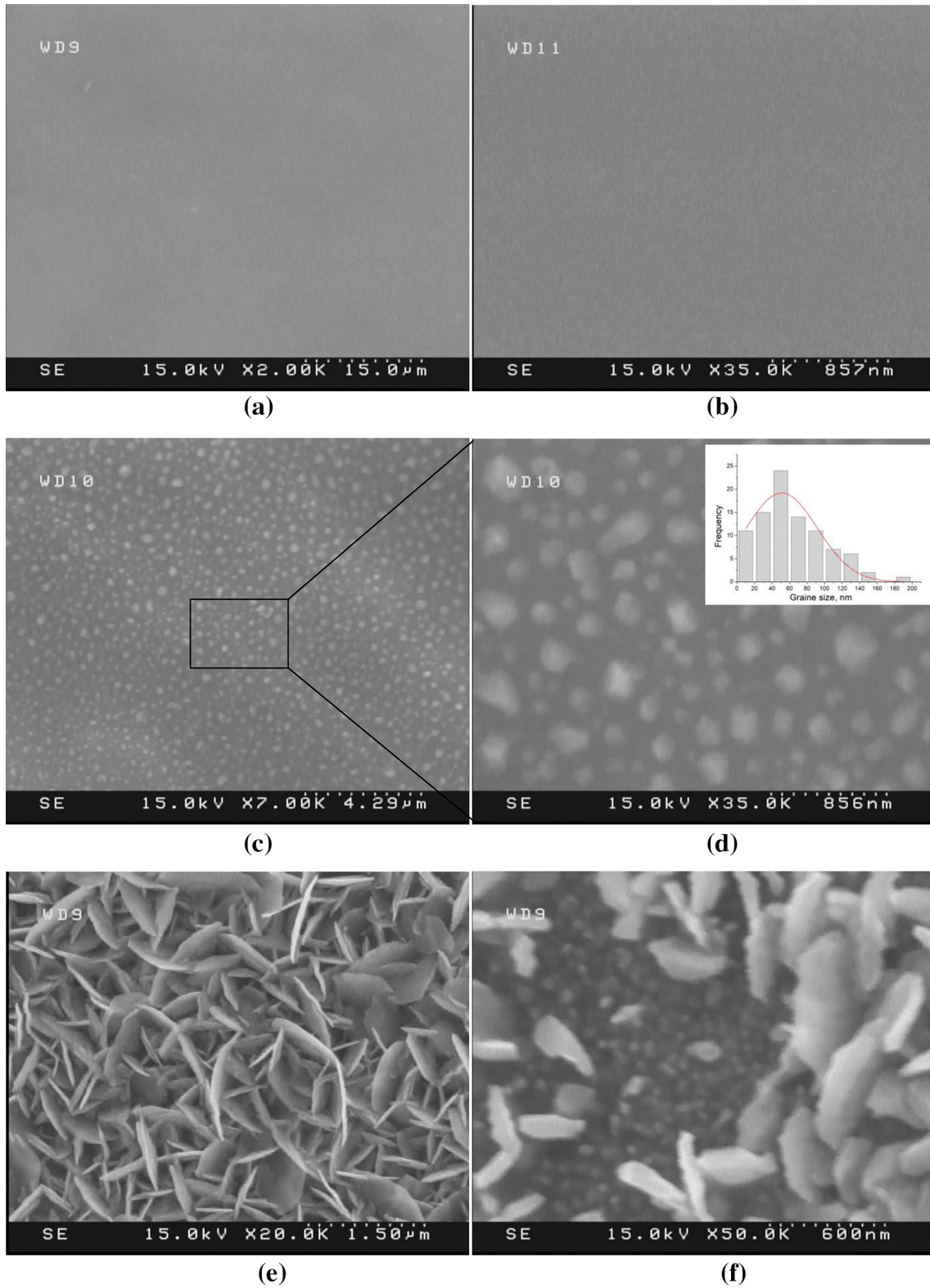
Fig. 6 FE-SEM images of the samples as-quenched (**a**) and (**b**) and annealed by Joule-heating technique under 1.9 V (**c** and **d**) and 2.1 V (**e** and **f**) during 20 s
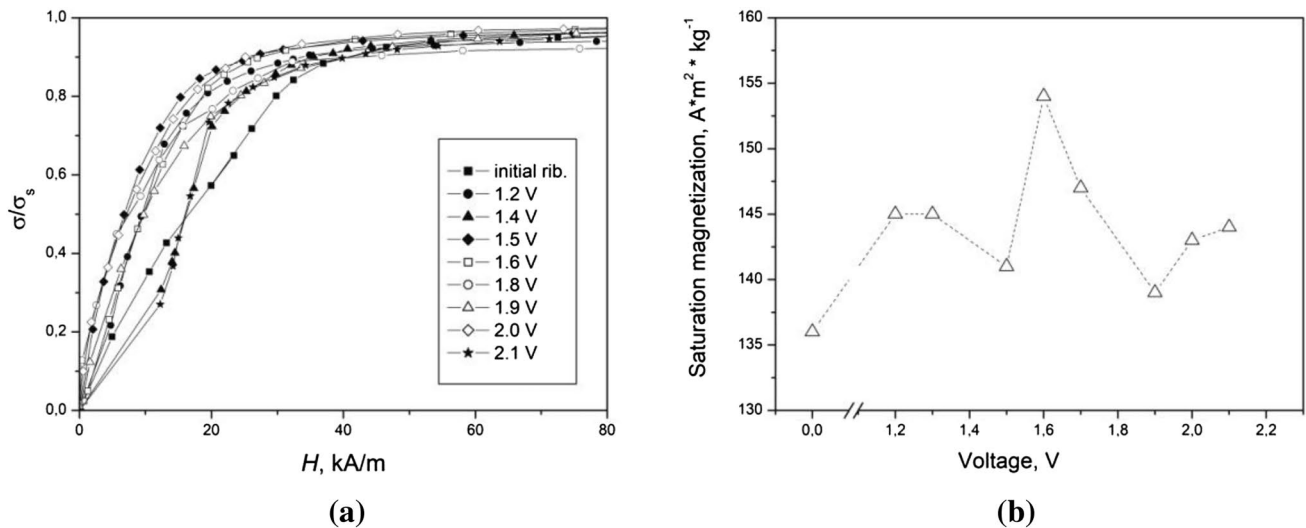
Fig. 7 Initial magnetization curves (**a**) and saturation magnetization as a function of applied voltage (**b**)

Conclusions

The features of Joule-heating on structure parameters of $Fe_{73.5}Nb_3Cu_1Si_{15.5}B_7$ amorphous ribbon were studied using the backscattered X-ray diffraction method, and the conditions for the formation of a fully or partially crystalline structure with nanograins of Fe_3Si and H-phase was determined. It is shown that Joule-heating technique can be used as an effective method for nanostructuring of amorphous alloys, including the formation of a 3D petal-like surface nanostructures. The crystallization behaviour of $Fe_{73.5}Nb_3Cu_1Si_{15.5}B_7$ ribbon depending on annealing duration was investigated and the Avrami exponent was obtained as $n = 0.82$.

It is shown that by changing the duration of annealing and the current density, it is possible to effectively vary the content and composition of crystalline phases, thus controlling the physical properties, increasing the microhardness and saturation magnetization. It can be concluded that optimal parameters of current annealing for $Fe_{73.5}Nb_3Cu_1Si_{15.5}B_7$ alloy properties optimization are current density of about 19–$20 *10^6$ A/m^2 and annealing duration of 20–60 s.
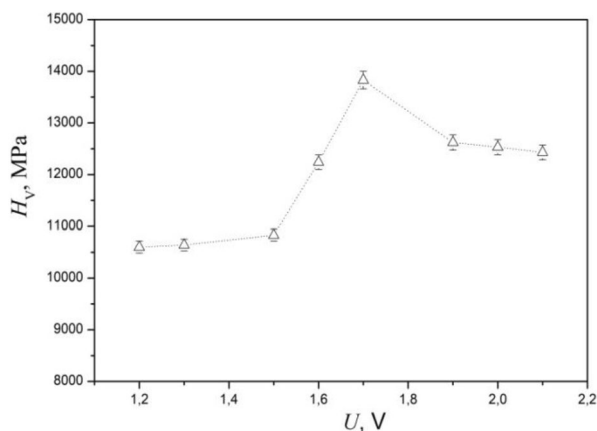
Data Availability The data will be available on the request.

Declarations

Conflict of interest The authors declare no conflict of interest.

Ethical approval This article does not contain any studies with human participants or animals performed by any of the authors.

References

Ackland K, Masood A, Kulkarni S, Stamenov P (2018) Ultra-soft magnetic Co-Fe-B-Si-Nb amorphous alloys for high frequency power applications. AIP Adv 8(5):056129. https://doi.org/10.1063/1.5007707

Allia P, Barricco M, Knobel M, Tiberto P, Vinai F (1994) Soft nanocrystalline ferromagnetic alloys with improved ductility obtained through dc Joule-heating of amorphous ribbons. J Magn Magn Mater 133(1–3):243–247. https://doi.org/10.1016/0304-8853(94)90536-3

Barandiaran J (2003) Kinetic aspects of nano-crystallization in Finemet-like alloys. J Non-Cryst Solids 329(1–3):57–62. https://doi.org/10.1016/j.jnoncrysol.2003.08.013

Fig. 8 Microhardness as a function of applied voltage

Bednarčík J, Cesnek M, Sovák P (2020) Soft magnetic amorphous alloys in X-ray light: Insights from ultra-fast Joule-heating experiments. J Magnet Magnet Mater 499:166282. https://doi.org/10.1016/j.jmmm.2019.166282

Boichyshyn L, Danyliak MO, Kotur B, Mika T (2017) The kinetic peculiarities of the nanocrystallization of amorphous alloys Fe84Nb2B14, which are doped by rare earth metals. Phys Chem Solid State 18(1):122–128. https://doi.org/10.15330/pcss.18.1.122-128

Cai Y, Xu J, Guo Y, Liu J (2019) Ultrathin, polycrystalline, two-dimensional Co3O4 for low-temperature CO oxidation. ACS Catal. https://doi.org/10.1021/acscatal.8b04064

Fanfoni M, Tomellini M (1998) The Johnson-Mehl- Avrami-Kohnogorov model: a brief review. Nouv Cim D 20:1171–1182. https://doi.org/10.1007/BF03185527

Gupta P, Gupta A, Franco V, Conde A (2007a) Joule-heating as a technique for obtaining uncoupled soft and hard magnetic phases in a Finemet alloy. J Appl Phys 101(3):033909. https://doi.org/10.1063/1.2432480

Gupta P, Gupta A, Principi G, Maddalena A, Bernstorff S, Amenitsch H (2007b) Effect of annealing current density on the microstructure of nanocrystalline FeCuNbSiB alloy. J Appl Phys 101(5):053907. https://doi.org/10.1063/1.2450676

Hasegawa R (2004) Applications of amorphous magnetic alloys. Mater Sci Eng, A 375–377:90–97. https://doi.org/10.1016/j.msea.2003.10.258

Imafuku M, Sato S, Koshiba H, Matsubara E, Inoue A (2000) Crystallization behavior of amorphous Fe90-xNb10Bx (x=10 and 30) alloys. Mater Trans, JIM 41(11):1526–1529

Jifeng Z, Junhua Y, Keqiang Q (2022) Advances in Fe-based amorphous/nanocrystalline alloys. J Appl Phys 132:040702. https://doi.org/10.1063/5.0092662

Kumar M, Bhatt V, Yun J-H (2020) Hierarchical 3D micro flower-like Co3O4 structures for NO2 detection at room temperature. Phys Lett A. https://doi.org/10.1016/j.physleta.2020.126477

Kyryliv Y, Kyryliv V, Tsizh B et al (2022) Resistance of surface nanostructures and ultrafine grain structures on steel 40Kh to wear and cavitation-erosive destruction. Appl Nanosci 12:1085–1090. https://doi.org/10.1007/s13204-021-01751-5

Langford JI, Wilson AJC (1978) Scherrer after sixty years: a survey and some new results in the determination of crystallite size. J Appl Cryst 11:102–113

Lashgari HR, Chen Z, Liao XZ, Chu D, Ferry M, Li S (2015) Thermal stability, dynamic mechanical analysis and nanoindentation behavior of FeSiB(Cu) amorphous alloys. Mater Sci Eng, A 626:480–499. https://doi.org/10.1016/j.msea.2014.12.097

Ma Y, Yang W, Pei J, Li H, Lu H, Liu H, Li M, Li W, Sun X, Li J, Inoue A (2022) Mechanism of low thermal conductivity for Fe76Si13B8Nb2Cu1 amorphous and nanocrystalline alloys at room temperature. J Non-Cryst Solids. https://doi.org/10.1016/j.jnoncrysol.2021.121264

Málek J (1995) The applicability of Johnson–Mehl–Avrami model in the thermal analysis of the crystallization kinetics of glasses. Thermochim Acta 267:61–73. https://doi.org/10.1016/0040-6031(95)02466-2

Mitra A, Palit S, Chattoraj I (1998) Crystallization and magnetic behaviour of Fe-Nb-Cu-Si-B alloys. Philos Mag B 77(6):1681–1691. https://doi.org/10.1080/13642819808206413

Mudry S, Kulyk Y, Tzizh B (2010a) Isothermal crystallization kinetics in Fe73.1Si15.5B7.4Nb3Cu1 amorphous alloy. Rev Adv Mater Sci 23:147–151

Mudry S, Kulyk Yu, Tsizh B (2010b) Isothermal crystallization kinetics in Fe73.1Si15.5B7.4Nb3.0Cu1.0 amorphous alloys. Rev Adv Mater Sci 23:147–151

Mudry S, Shtablavyi I, Liudkevych U, Winczewski S (2015) Structure and thermal expansion of liquid bismuth. Mater Sci-Pol 33(4):767–773. https://doi.org/10.1515/msp-2015-0100

Mudry S, Kulyk Y, Korolyshyn A (2007). Plevachuchuk temperature dependence of structure of amorphous Fe73.1Si15.5B7.4Nb3Cu1 Alloy. Rev Adv Mater Sci 14:41–45

Nosenko VK, Maslov VV, Kirilchuk VV, Kochkubey AP (2008) Some industrial applications of amorphous and nanocrystalline alloys. J Phys Confer Ser. https://doi.org/10.1088/1742-6596/98/7/072016

Nosenko VK (2015) Amorphous and nanocrystalline alloys for instrument making and energy efficient technologies Visnyk of the National Academy of Sciences of Ukraine 4

Nykyruy YS, Mudry SI (2020) Chapter 6. Effect of laser irradiation on the structure of IRON based amorphous alloys. In: Wythers MG (ed) Advances in materials science research, vol 40. Nova Science Publishers, New York, pp 189–228

Nykyruy YS, Mudry SI, Kulyk YO, Lapinski M (2020) Nanocrystallization and phase formation in Fe73.5Nb3Cu1Si15.5B7 amorphous ribbon under laser heating. Mater Sci Pol 38(4):526–534. https://doi.org/10.2478/msp-2020-0064

Nykyruy Y, Mudry S, Kulyk Y et al (2022) Magnetic properties and nanocrystallization process in Co–(Me)–Si–B amorphous ribbons. Appl Nanosci. https://doi.org/10.1007/s13204-022-02746-6

Nykyruy YS, Mudry SI, Kulyk YO, Zhovneruk SV (2018) Structural transformation in Fe73.5Nb3Cu1Si15.5B7 amorphous alloy induced by laser heating. Lasers Manuf Mater Process 5(1):31–41. https://doi.org/10.1007/s40516-017-0051-1

Ohnuma M, Sasaki O, Kuwano H, Katano S, Morii Y, Funahashi S et al (1993) Crystallization process of Fe80P20−xSix Amorphous. Alloys Mater Trans JIM 34(10):874–881. https://doi.org/10.2320/matertrans1989.34.874

Okulov I, Soldatov I, Sarmanova M et al (2015) Flash Joule-heating for ductilization of metallic glasses. Nat Commun 6:7932. https://doi.org/10.1038/ncomms8932

Parveen N, Cho MH (2016) Self-assembled 3D fower-like nickel hydroxide nanostructures and their supercapacitor applications. Sci Rep. https://doi.org/10.1038/srep27318

Paul T, Loganathan A, Agarwal A, Harimkar SP (2018) Kinetics of isochronal crystallization in a Fe-based amorphous alloy. J Alloy Compd 753:679–687. https://doi.org/10.1016/j.jallcom.2018.04.133

Plevachuk Y, Sklyarchuk V, Khalouk K, Gasser J (2014) Electrical resistivity and thermoelectric power of ternary Fe–Si–B alloys. Visnyk of the Lviv University. Ser Phys 2014(49):21–28

Pogorily AM, Polishchuk DM, Tovstolytkin AI, Kravets AF, Zamorskyi VO, Nosenko AV, Nosenko VK (2019) Resonance properties and magnetic anisotropy of nanocrystalline Fe73Cu1Nb3Si16B7 alloy. Ukrain J Phys 64(10):942. https://doi.org/10.15407/ujpe64.10.942

Rezaei-Shahreza P, Seifoddini A, Hasani S (2017) Thermal stability and crystallization process in a Fe-based bulk amorphous alloy: the kinetic analysis. J Non-Cryst Solids 471:286–294. https://doi.org/10.1016/j.jnoncrysol.2017.05.044

Shi L, Qin X, Yao K (2020) Tailoring soft magnetic properties of Fe-based amorphous alloys through C addition. Progr Nat Sci Mater Int. https://doi.org/10.1016/j.pnsc.2020.02.001

Shihab MT, Reza MA, Shil SK, et al (2020) Study of crystallization phases and magnetic properties of Fe72.5Cr1 Nb3 Cu1 Si13.5B9 nanocrystalline alloy prepared by rapid quenching method. Mater Sci Eng 4(2):37−43. https://doi.org/10.15406/mseij.2020.04.00124

Sun X, Cabral-Prieto A, Jose Yacaman M, Reyes-Gasga J, Hernandez-Reyes R, Morales A, Sun W (2000) Nanocrystallization behavior and magnetic properties of amorphous Fe78Si9B13 ribbons. Physica B 291(1–2):173–179. https://doi.org/10.1016/s0921-4526(99)01241-7

Svoboda R (2021) Crystallization of glasses—when to use the Johnson–Mehl–Avrami kinetics? J Eur Ceram Soc 41(15):7862–7867. https://doi.org/10.1016/j.jeurceramsoc.2021.08.026

Wang Y, Zhang Y, Takeuchi A, Makino A, Kawazoe Y (2016) Investigation on the crystallization mechanism difference between FINEMET® and NANOMET® type Fe-based soft magnetic amorphous alloys. J Appl Phys 120(14):145102. https://doi.org/10.1063/1.4964433

Bhosale Sheshanath V, Kobaisi Mohammad Al, Jadhav Ratan W, Jones Lathe A (2021) Flower−Like superstructures: structural features applications and future perspectives. Chem Rec 21(2):257–283. https://doi.org/10.1002/tcr.202000129

Sheng X, Wang L, Chen G, Yang D (2011) Simple synthesis of flower-Likeln2S3Structures and their use as templates to prepare CuS particles. J Nanomaterials 2011:1–5. https://doi.org/10.1155/2011/280216